Synthesis, characterization, and biological activity of silver nanofibers essential oils of prunus dulcis

Nuha A.M. Obaid[a], Noor H. Faisal[a], Nuha W. Ali[a], Ruaa G. Ibrahim[a], Ayat N. Hassan[a], Ayat J. Kadhum[a], Ali A.A. Al-Shawi[a], Mohammed E. Mohmmed[a], Mohnad Abdalla[b]

[a]Department of Chemistry, College of Education for Pure Sciences, University of Basrah, Basrah, Iraq, [b]Pediatric Research Institute, Children's Hospital Affiliated to Shandong University, Jinan, Shandong, China

Correspondence to Mohnad Abdalla, PhD, Pediatric Research Institute, Children's Hospital Affiliated to Shandong University, Jinan, Shandong 250022, China.
Tel: +249125215381;
e-mail: mohnadabdalla200@gmail.com

Background

Prunus dulcis possesses various beneficial qualities, including liver-protective, cardio metabolic, antimicrobial, anti-inflammatory, and anxiety-reducing properties. Furthermore, the oil is a fantastic moisturizing cream for hair and skin, to it can help prevent stretch marks and ultraviolet-visible spectroscopy damage. These biological applications highlight the importance of developing nanotechnology applications for *P. dulcis* almond oils.

Materials and methods

In this study, essential oils derived from the fruit of the almond tree (*P. dulcis*) were employed as reducing agents for producing silver nanofibers (AgNFs). Synthesized AgNFs were characterized using ultraviolet-visible spectroscopy, scanning electron microscopy, and Fourier transform infrared spectroscopy. The biological activities of (AgNFs) were examined.

Results

The current study showed the absorption of synthesized (AgNFs) at 415 nm. Scanning electron microscopy analysis showed the nanofibers average diameter varied from 200 nm to 10 nm. The biological activities of (AgNFs) were evaluated using minimum inhibitor concentration, half-maximal inhibitory concentration (IC_{50}), and flow cytometry tests. The cell cycle test of (AgNFs) showed it arrested with S-phase of two types of human cancer cells (HepG2 liver cancer cells and MDA-MB-231 breast cancer cells).

Conclusion

These antibacterial and anticancer properties of AgNFs highlight the increased medicinal value of essential oils when coupled with AgNFs produced from almond essential oil.

Introduction

Nanotechnology and nanoparticles are prized for their small size and high surface area to volume ratio, which improves chemical, mechanical, magnetic, and optical characteristics [1]. These properties lead to their well-established biomedical applications, including using antioxidant substances, antimicrobial agents, and chemotherapeutic medicines [2,3]. Further investigation into green techniques is critical for increasing the usage of metal nanoparticles in a wide range of applications. Biosynthesis approaches that use microbes, algae, and plants are considered innovative for generating metal nanoparticles [4,5] Metallic nanoparticles, such as gold, silver, zinc, platinum, copper, and iron, have attracted substantial attention because of their numerous biological properties, including anticancer, antibacterial, and medicine delivery abilities, making them valuable for different biomedical applications [6]. Because of their unique properties, including thermal and electric conductivity and antibacterial activity, silver nanoparticles in particular have become commonplace in various industries [7]. Nanoparticles can be produced using a variety of processes, including chemical reduction, electrical reduction, electrospinning, and photochemical reaction reduction. Electrospinning yields nanofibers, whereas reduction yields nanoparticles. The technique utilized to generate nanoparticles is crucial since it impacts their shape, size, stiffness, and chemical and physical properties [8,9]. Nanofibers have outstanding properties such as surfaces with pores, small fiber diameters, and a high surface-to-volume ratio [10]. Several researches have

examined the potential uses of nanofibers and addressed challenges in certain fields, such as effective medicine administration [11,12], wastewater purification and treatment [13], oxygen electro catalysis [14], electronic and energy applications [15], water splitting [16], smart food packaging [17], extraction of solid phases in liquid separation [18], and sustainable uses [19]. Cancer is among the main causes of death in the globe. Despite advances in drug research, most modern drug-targeted therapy are extremely expensive and linked with substantial side effects and morbidity. There is a pressing need to identify new plant-derived. Indeed, the design and development of chemopreventive agents that act on specific and multiple molecular and cellular targets is gaining support as a rational approach to prevent and treat cancer. Several medicinal plant extracts (*Portulaca oleracea*, *Allium sativum*, *Rheum palmatum*, *Salvia officinalis*, *Geranium robertianum*, *Rosmarinus officinalis*, *Calendula officinalis*, etc.) have been demonstrated to exhibit anti-cancer activity on numerous human cancer cells [20,21]. Essential oils are natural, organic substances that are both secure green, aromatic, volatile compounds derived from various plant parts such as flowers, seeds, buds, stems, roots, leaves, wood, and bark. However, the hydrophobic nature of essential oils may be an obstacle to the synthesis of nanoparticles; consequently, an aqueous solution of silver salt is used as a silver precursor for synthesis. Studying the efficacy of nanoparticles controlled by essential oils is required to identify the critical features required to produce stable particles [22,23]. Almonds contain healthy fats such as linoleic acid, oleic acid, and palmitic acid, among others. It also contains some antioxidants, such as vitamin E and phenolic compounds, which contributes to its widespread application in medicine for various health benefits [24,25]. Almond oil is an abundant resource of antioxidants, oleic acid (64–82%), and vitamin E (240–440 µg/g), preventing free radical-induced cell damage and supporting their development and survival. This oil has minimal blood compatibility and toxicity, making it a good part of a medication formulation [26–28]. The oil from almonds is a healthy fat that can be used to improve the nutritional value of a variety of foods [29]. Various fatty acids, or vegetable oils, have recently been used as stabilizers [30]. The biological activities of almond oil nanoparticles were highlighted in research on their synthesis, increasing the likelihood of future applications [31]. These developments are based on nanotechnology techniques that emphasize medical applications in a variety of sectors [32,33]. According to the abovementioned oil properties, this study aimed to produce AgNFs utilizing almond oil. The shape of AgNFs was investigated by a scanning electron microscope (SEM), ultraviolet-visible spectroscopy, and Fourier transform infrared (FT-IR). AgNFs' antibacterial activity was tested against *Pseudomonas aeruginosa* and *Escherichia coli*, and their anticancer properties were investigated.

Materials and methods

Silver nitrate ($AgNO_3$) was purchased from Merck (Germany). *Prunus dulcis* is planted in North Iraq, where the climate is ideal for growing through in cold environments in mountainous areas and the soil is not salty. The fruit was cleaned, cut into small bits, milled, and stored in 4°C opaque glass containers until needed.

Essential oil isolation method of *p. dulcis*

We adopted the Zakeri *et al.* [34] method for isolating essential oil from *P. dulcis* fruit using a water solvent. 10 g of *P. dulcis* powder was combined with 300 ml of water distilled in a Clevenger apparatus for 3 h, and essential oil was collected from the condenser.

Synthesis of silver nanofibers (AgNFs)

1 mM $AgNO_3$ solution was prepared by adding 0.1699 g of $AgNO_3$ to 1 l distilled water. 90 ml of freshly prepared 1 mM $AgNO_3$ solution and 9 ml of almond oil were combined in a conical flask to make a $AgNO_3$ solution. The reaction was then vigorously performed on a hot plate with a magnetic stirrer inside the flask. At 14 min, the biosynthesis reaction began, and the color reaction was observed, revealing that the clear $AgNO_3$ solution had changed to a light brown color, suggesting the creation of silver nanofibers (AgNFs) [35].

UV-Visible spectra

The UV-visible spectra of silver nanoparticle citral 1 mM were measured using a Labomed UVD-2950 UV-VIS Double Beam PC.A 2 nm resolution scanning spectrophotometer. This means it employs light in the visible and nearby regions (near-UV and NIR). The absorption of chemicals in the visible spectrum has a direct impact on how we perceive colors. In this region of the optical spectrum, molecules undergo electrical transitions.

Fourier –transform infrared spectroscopy (FT-IR)

Fourier transforms were employed to examine the infrared (Shimadzu, Kyoto, Japan) spectrum of biogenic nanomaterials that had been created. To detect the location of biological entities involved in

particle formation, AgNFs that are biogenic with KBr crystals were employed as the beam splitter. After centrifugation for 10 min at 8000 rotations per min, the pellets were dried at 80°C and crushed to remove unwanted plant materials and KBr crystals. The AgNFs spectra were acquired using a machine range of 400–4000 cm^{-1}.

Scanning electron microscopy (SEM) analysis

SEM images of AgNFs were taken employing a JSM-JEOL 6390 SEM microscope. The JSM-6390 is an outstanding performance, inexpensive scanning electron microscope. The customized graphical user interface makes the instrument easy to operate. It includes an auto coater for covering the sample after AgNFs were sputtered with platinum and evenly placed on the container for the sample with carbon tape. SEM pictures were collected to figure out the existence of the essential parts of the nanoparticles in the sample at various intervals.

Antibacterial evaluation of silver nanofibers (AgNFs)

E. coli ATCC 25922, as well as *p. aeruginosa ATCC 27853*, were used as microbial strains. The Clinical Laboratory Standard Institute (CLSI) determines minimum inhibitory concentrations (MICs) as the smallest level of concentrations for each tested drug needed to limit the visible growth of the tested bacteria. Every chemical was divided twice in series on sterile micro-dilution plates with Mueller Hinton broth media at concentrations ranging from (0.003 to 4) ml. Following that, bacteria expulsions in clean, normal saline were prepared and modified to a McFarland standard of 0.5 turbidity. The solution was reduced (1 : 100) in sterilized Mueller-Hinton broth (MHB) shortly before it was added to the trays containing multiple dilutions of each component. A total of 10^6 bacterial cells were used to test each dose. 96 well plates were kept warm at 37°C for 24 h. 10 ml of sterile distilled water and 4 mg/ml of the reagent base solution were put into each well. Tetracycline was employed as an ordinary antibiotic against bacterial strains in every one of the tests, which were conducted in triplicate. Minimum Bactericidal Concentration (MBC) was calculated by incubating 100 µl of each of the no-growth wells (concentration) for 24 h at 37°C on a nutrient agar plate [36].

Anticancer evaluation of silver nanofibers (AgNFs)

Cells were cultured in RPMI-1640 (Gibco) and Dulbecco's Modified Eagle Medium (DMEM) (Gibco) media with 10% Fetal Bovine Serum (FBS) and medicines (100 g /ml amoxicillin and 100 g/ml streptomycin). Cells were transmitted at 37°C in hydrated air containing 5% CO_2 with trypsin/EDTA (Gibco) and a phosphate-buffered solution of saline. MTT [3-(4, 5-dimethylthiazol-2-yl)-2, 5-diphenyltetrazolium bromide] assays (Sigma-Aldrich) were used to determine the development of cells and survival. Trypsin-digested cells were collected, adjusted to a cell density of 1.4×10^4 cells/well, and grown in 96-well plates with 200 µl of new media per well for 24 h. Following forming a monolayer, the stem cells were treated for 24 h at 37°C with 5% CO_2 in 100–6.25 µg/ml of the sample. The dish was incubated at 37°C for a further four hours with the MTT solution (the cytoplasm of cells was removed and dimethyl sulfoxide (100 µl per well) was added) after the supernatant was removed at the end of the treatment (24 h). Shaking the cells at 37°C allowed the granules to disintegrate entirely. Cell viability was measured at 570 nm absorbance using an enzyme-linked immunosorbent assay (ELISA) reader (the model raised is xs2, Bio Tech (USA). Dose-response curves were used to determine the amount of chemicals causing 50% mortality in cells (IC_{50}) [37].

Reactive oxygen species (ROS) assay

Production of ROS was measured using the flow cytometry technique and 2′, 7′ dichlorodihydro fluorescindiacetate (DCFH2-DA) (Sigma-Aldrich). Easy to enter cells, this dye is removed by within-cells esterase to create 2′, 7′ dichlorodihydrofluorescin (DCFH2), which becomes lodged inside the cells. Highly visible 2′, 7′-dichlorofluorescein (DCF) is created by the oxidation of DCFH2 by hydrogen peroxide or low-molecular-weight peroxides generated by the cells. As such, the luminosity intensity is proportional to the amount of peroxide produced by the cells from hydrogen. Cells (1×10^5 cells/well) were treated with the compound at its IC_{50} concentration for 12 h. Following treatment, the cells were harvested, and centrifuged at 1500×g for 5 min, and the pellet was washed with 1 ml of phosphate-buffered saline (PBS). After washing, the cells were incubated with 20 µM DCFH-DA (2′,7′-dichlorofluorescin diacetate) in the dark for 30 min. Fluorescence was then measured using a flow cytometer, with excitation and emission wavelengths set at 485–495 nm and 525–530 nm, respectively. Data were collected in the FL1 channel to assess the level of reactive oxygen species (ROS) [38].

Cell cycle phase analysis

HepG2 and MDA-MB-231 cells (3.5×10^5 cells each) were treated with the IC_{50} concentration of AgNFs for 24 h. After treatment, the cells were washed with 1 ml of PBS, centrifuged at 1500×g for 5 min at 4°C, and

then fixed with 70% ethanol at 4°C for 24 h. Following fixation, the cells were centrifuged again to remove the ethanol and re-suspended in PBS for 30 min. The pellet was then treated with 20 µg/ml ribonuclease A (RNase) (Sigma-Aldrich) and 20 µg/ml propidium iodide (PI) (Sigma-Aldrich). Cell cycle stages were analyzed using flow cytometry, and data were processed with FlowJo software version 7.6.1 [39].

Detection of apoptosis by annexin V-fluorescein isothiocyanate (V-FITC) and propidium iodide (PI) staining

We used the BioVision Annexin V-FITC apoptosis kit to detect dead and apoptotic HepG2 and MDA-MB-231 cells that had received AgNF injections. Cells were collected, carefully washed, and labeled with FITC and PI one day after being treated with the AgNFs IC_{50} concentration. 5×10^5 cells were gathered and centrifuged (1500×g for 10 min) with neglected control cells after receiving treatment with NA IC_{50} concentration for 24 h. The FL1 indicator detector identified PI-stained cells, but not the FL3 signal detector to be tested. After recovering the fragment in 500 µl of 1X attachment buffer, 5 µl of annexin V-FITC and 5 µl of a 50 µg/ml PI solution were added and left for 5 min at room temperature. The tagged cells were examined after incubation using Partec PAS, Germany, fluorescence-activated cell sorting analysis equipment. Signals were gathered from PI-stained cells using an FL3 signal detector to determine the arrangement of cells that had been labeled differently and from annexin V-FITC cells that had been labeled using a FITC signal detector (FL1) [40].

Statistical analysis

The IC_{50} is calculated in the Excel file using the dose-response curve. The absorbance at 570 was recorded at each concentration. The absorbance is used to calculate the viability percentages for each concentration. The average viability and standard deviation are computed. The curve was created, and the equation about the graph was derived and shown in the graph's right corner. The equation produces the values a and b needed to calculate the IC_{50}.

Results and discussion

The UV-visible spectra

The UV-visible spectrum for AgNFs made from almond essential oils is shown in (Fig. 1). The mixture of almond essential oil and $AgNO_3$ color change. This showed that ions were reduced, which proved the formation of silver nanoparticles. The spectrum has a peak at 415 nm, which is caused by the Plasmon absorption of metallic silver nanoparticles. The results fit with what these studies found by Vijayan et al., [41]. These studies showed that the color change was caused by silver ions being reduced to silver metals.
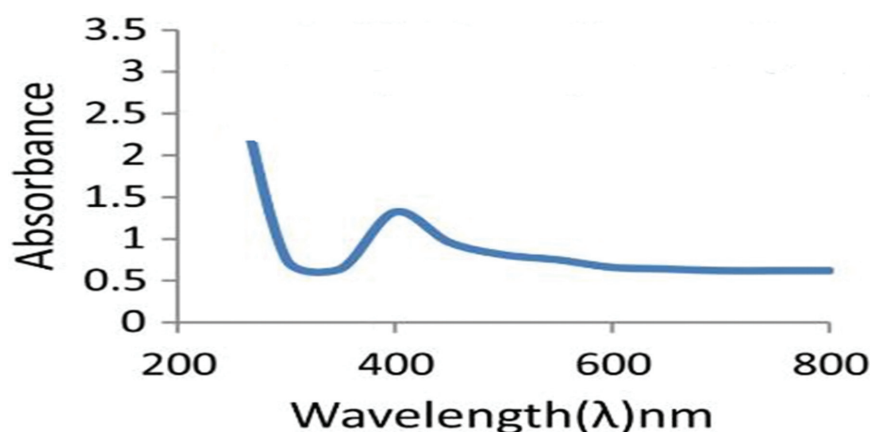
FT-IR analysis

Figure 2 depicts the FT-IR spectrum of unrefined oil from almonds and AgNFs in the form of almond oil, with revealing bands corresponding to olefinic double-bonded bands (3085.42 cm^{-1}), members of the methylene group (2926.33, 2855.05, 1464.13, and 723.65 cm^{-1}), a methyl group (1464.13 and 1377.28 cm^{-1}), and the triglyceride ester groups (1744.32, 1166.31, and 864.11 cm^{-1}). Because of the Plasmon effect of the nanoparticles, sharper peaks in the instance of AgNFs in almond oil [42–44].
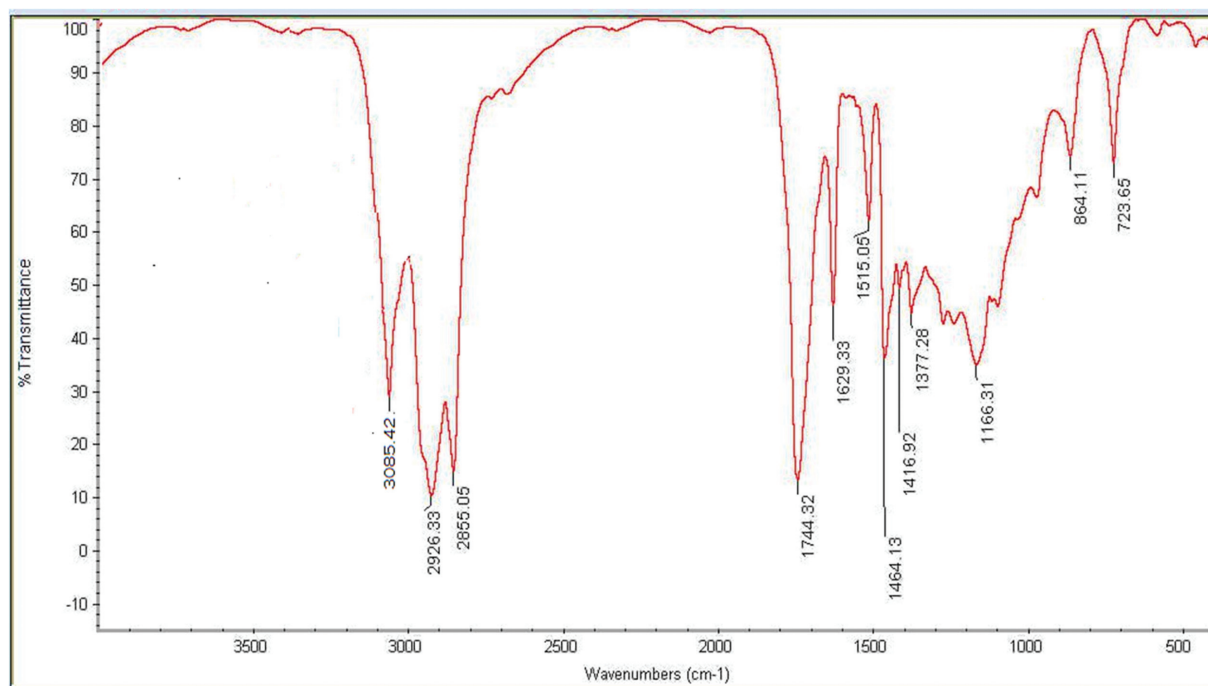
SEM analysis

SEM was employed to analyze the morphology of biosynthesized AgNFs at different resolutions of 200 nm. It additionally serves to calculate the particle size. The SEM results of AgNFs involved in the sizes and shapes are depicted in (Fig. 3). AgNFs formation of fiber morphology is found to have an

Figure 1

UV-Vis spectrum of silver nanoparticles reduced by the oil co.
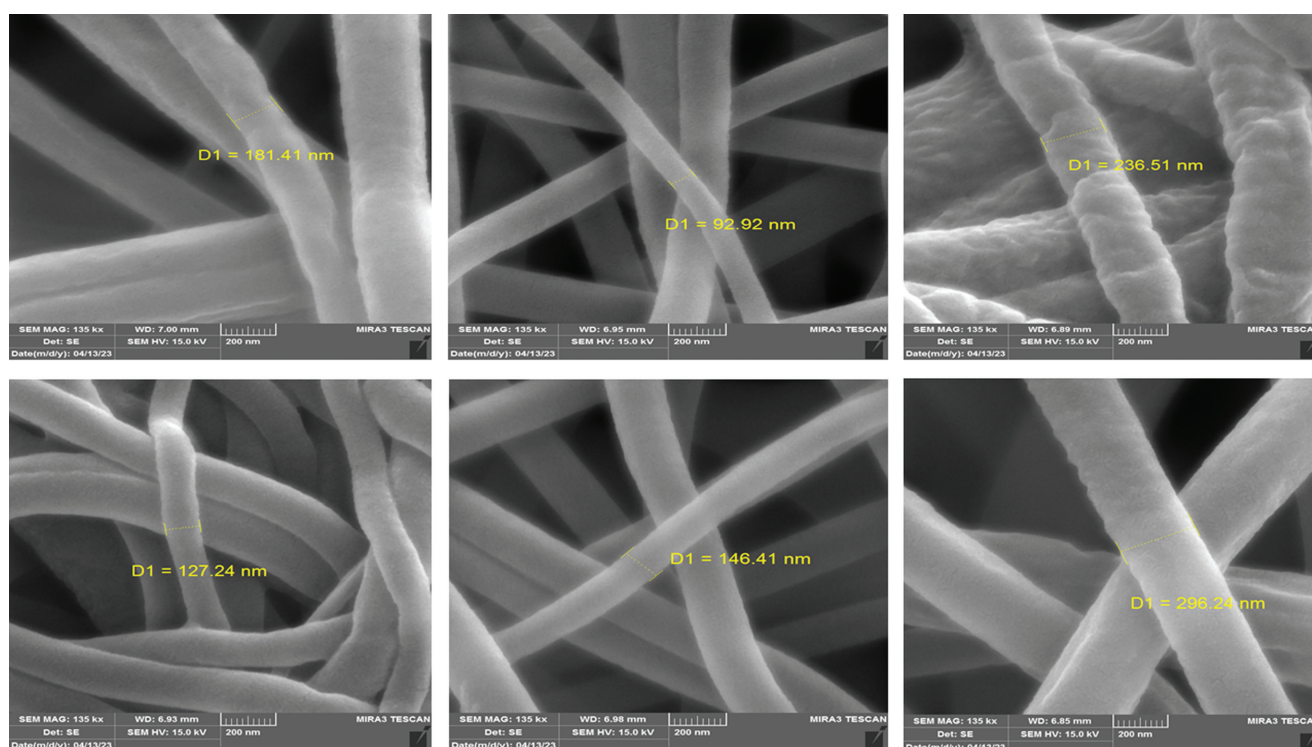
Figure 2

Fourier transform infrared spectroscopy spectra of silver nanofibers.

average length of 90 to 300 nm. Figure 3 clearly illustrates that increasing the concentration of plant extract increases the nanoparticle dimension. The average particle diameters of the samples were 92.92 nm, 127.24 nm, 146.41 nm, 181.41 nm, 236.51 nm, and 296.24 nm, according to SEM images. This study discovered that raising the concentration of extract increases particle size. Other

Figure 3

Scanning electron microscope image of silver nanofibers, which showed various nanofibers sizes (92.92–296.24) nm.

researchers have reported on this phenomenon as well. The average length of green-produced AgNFs demonstrates their utility for biotechnological and biological applications [45].

The antibacterial activity of silver nanofibers (AgNFs)

AgNFs have demonstrated biocidal properties against gram-negative microbes (*E. coli and P. aeruginosa*). Gram-negative microbes were less sensitive to AgNFs, as evidenced by decreased zones of inhibition and increased MIC and MBC values, Table 1. The result might be because of the thick peptidoglycan coating on gram-negative cell walls [46]. However, it is widely acknowledged that particle size, particle form, stabilizing agent, and dosage, as well as the duration of therapy, all affect AgNF antibacterial activity [47]. The method by which elemental AgNFs decrease bacterial activity is that when they interact with the bacteria's cell wall, the outermost layer of the nanoparticles emits Silver ions [48]. Because of the nanostructured matter size of metal atoms, changes in the surface's local electrical composition may improve the responsiveness of nanoparticle surfaces [49]. The activity of AgNFs on the cell may cause a response that results in cell death. Finally, AgNFs emit Silver ions, contributing to AgNF's bactericidal activity. The difference in antibacterial activity between AgNFs and *E. coli* was larger than between AgNFs and *P. aeruginosa*. This is related to the different susceptibilities to AgNFs, namely the thickness and composition of the bacteria's cell membrane. The biocidal effects of AgNFs may be attributed to the formation of ROS, which may destroy the biomolecular structure of bacterial membranes in cells [50].
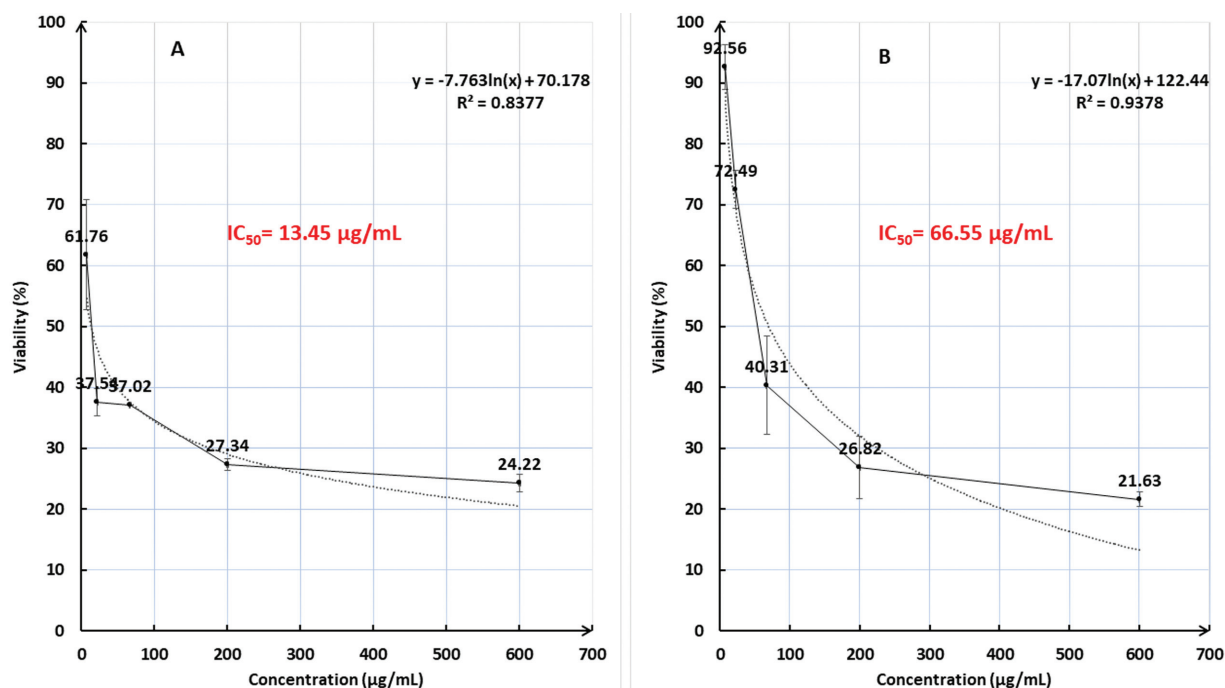
The anticancer0 activity of silver nanofibers (AgNFs)

Cancer medicines must meet two fundamental requirements: selective cytotoxicity and efficacy. A drug's ability to cause cancer cell apoptosis renders it an effective cancer treatment. Prospective drugs must not harm the immune cells since they fight cancer alongside the body's defenses. To comprehend these effects, silver nanoparticles have been investigated in HepG2 cancer cells and MDA-MB-231 cancer cells (Fig. 4a). HepG2 cell viability declined significantly at concentrations of 7.4, 22.22, 66.66, 200, and 600 µg/ml (corresponding to 61.76%, 37.54%, 37.02%, 27.34%, and 24.22% viability,

Table 1 The minimum inhibitor concentration and MBC values of the silver nanofibers against the microorganisms

Bacteria	AgNFs (µg/ml)	Tetracycline (µg/ml0)
E. 00coli		
MIC	0.34	8
MBC	0.48	16
P. 0aeruginosa		
MIC	0.24	1024
MBC	0.31	2048

Figure 4

Showed IC$_{50}$ values of silver nanofibers: A. IC$_{50}$ value of HepG2 equal to 13.45 µg/ml. B. IC$_{50}$ value of MDA-MB-231 cells equal to 66.55 µg/ml.
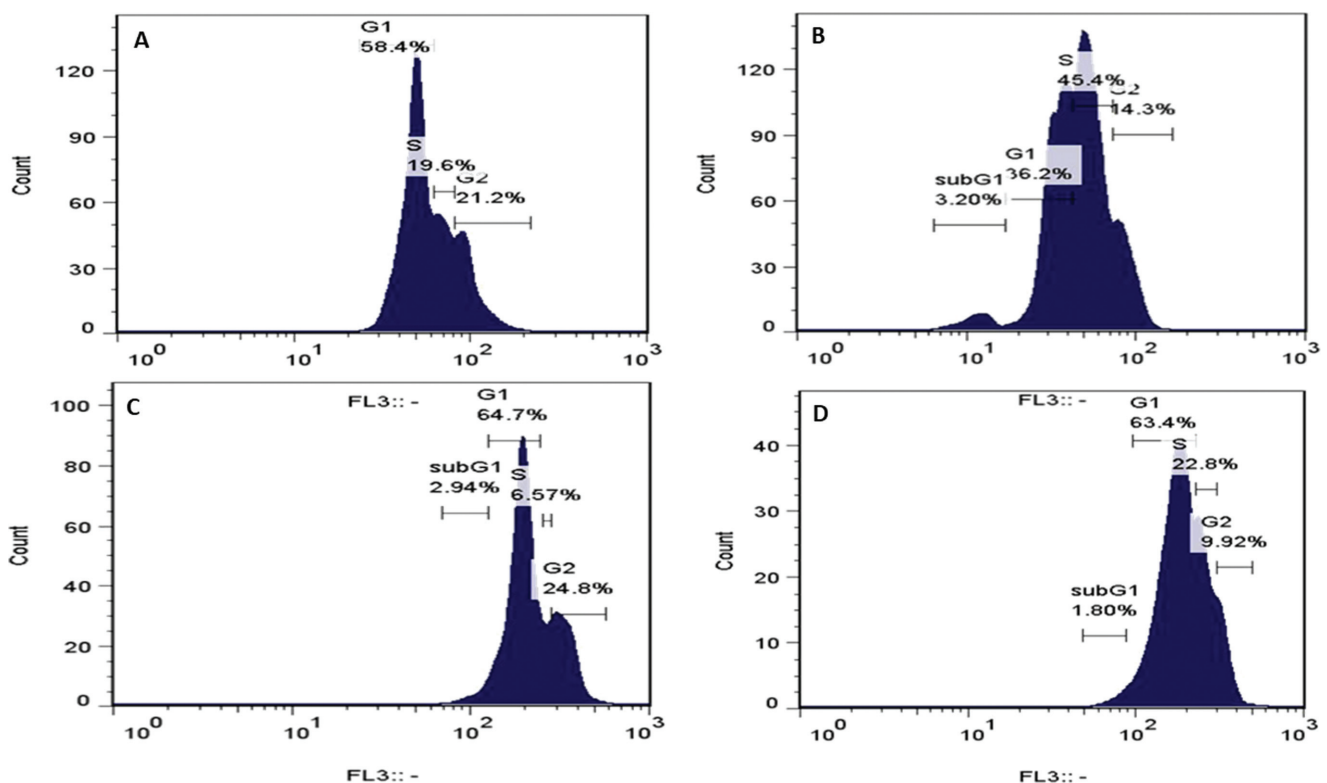
respectively). According to the findings of the MTT assay, the IC_{50} values were calculated using the Excel application the IC_{50} value for AgNFs was around 13.45 mg/ ml. Toxicity is negligible at lower doses, according to previous research. Figure 4b shows a significant decrease in MDA-MB-231 cell viability at the same concentrations (corresponding to 92.56, 72.49, 40.31, 26.82, and 21.63% vitality, respectively) the value of AgNFs' IC_{50} was found to have been 66.55 mg/ml. These results demonstrate that, in addition to murdering lines of cells, AgNFs cause a dose-dependent rise in cancer prevention effects. The low cytotoxicity of AgNFs has already been documented. In contrast, the AgNFs generated by Penicillium aculeate Su1 were found to be very biocompatible with normal human cells (HBE cells). Based on these findings, it is anticipated that the use of green manufacturing methods, such as various plant extracts and oils, will reduce the cytotoxic impacts. Using three experiments: cell cycle, reactive oxygen species, and apoptosis, we employed flow cytometry to identify potential AgNFs for further exploration against the HepG2 cancer cell and the MDA-MB-231 cancer cell [51,52].

Flow cytometry analysis
Cell cycle

The cell cycle is a three-step procedure that occurs inside the cell (G1, S, and G2) to understand the action and mechanism of plant extract. As a result of this procedure, plant extract may play a role. The IC_{50} value was used to target the checkpoint in this experiment. In (Fig. 5a and b), AgNFs would stop the life cycle of HepG2 cells when treated with half the inhibitory concentration (IC_{50} 13.45 µg/ml). It was found that AgNFs stop the cell life cycle at the G1 phase (at the S/G1 checkpoint), where it was observed. The statistical percentage of DNA content in the G1 phase decreased to 36.2% compared to the control at 58.4%. There was a significant decrease in the level of DNA spikes in the S phase to 45.4%, compared to 19.6% in control cells. Figure 5c and d show that in MDA-MB-231 cells, AgNFs stop the life cycle of MDA-MB-231 cells when treated with half the inhibitory concentration (IC_{50} 66.55 µg/ml). It was found that AgNFs The cell life cycle stops at the G1 phase (at the S/G1 checkpoint), where it was observed. The statistical percentage of DNA content at the G1 phase decreased to 63.4% compared to the control, 64.7%. There was a significant decrease in the level of DNA spikes in

Figure 5

Flow cytometry analysis of silver nanofibers, showed the cell cycle arrest analysis: A. Untreated HepG2 cells. B. HepG2 cells treated with IC_{50} value of silver nanofibers. C. Untreated MDA-MB-231 cells. D. MDA-MB-231 cells treated with IC_{50} value of silver nanofibers.
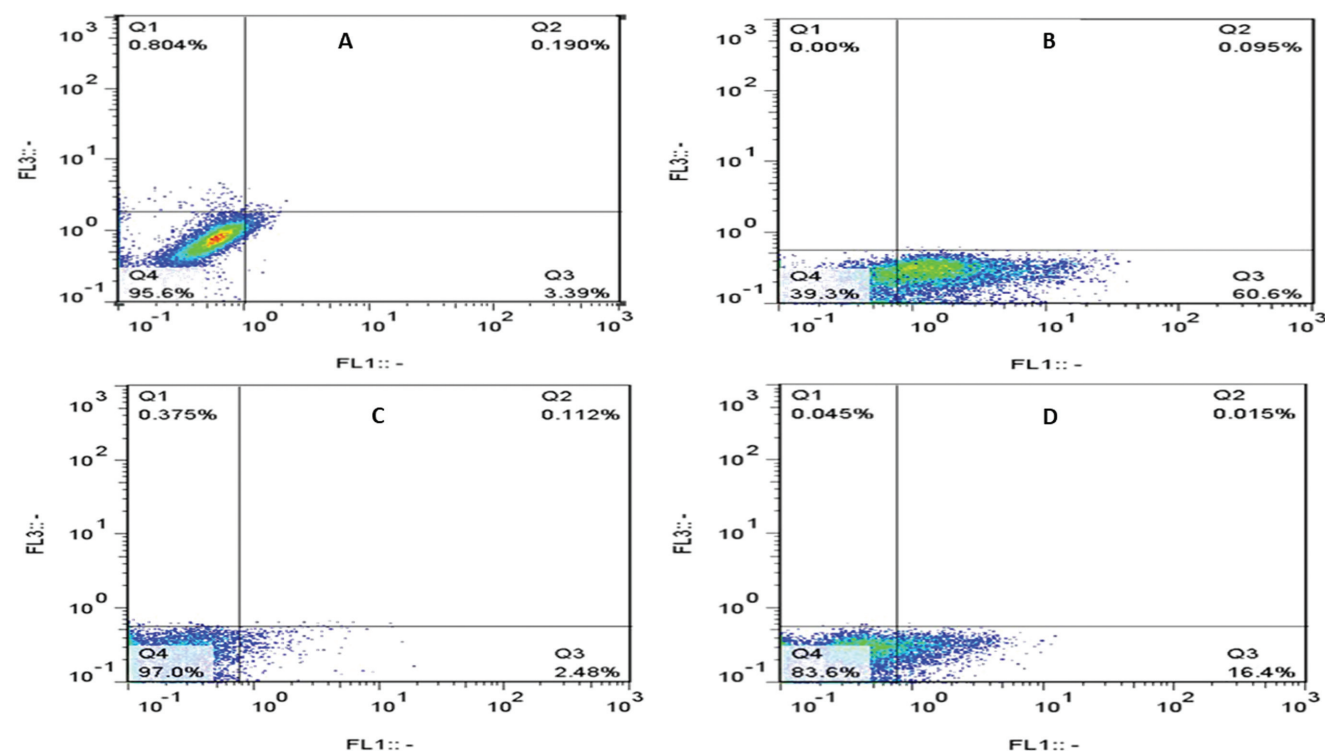
the S phase to 22.8% compared to 6.57% in control cells [53].

Apoptosis

To improve *P. dulcis* essential oil's anticancer activity and connect the findings to the cell cycle and ROS. We used an apoptotic assay to compare and contrast the efficacy of AgNFs against HepG2 cells and MDA-MB-231 cells. Apoptosis is a sort of programmed cell death that happens in eukaryotes, such as humans. It has been reported in both unicellular and multicellular eukaryotes, as well as in bacterial apoptotic processes. Membrane permeability changes during apoptosis, as seen by the collapse of the inner mitochondrial transmembrane potential. Chromatin condensation and nuclear fragmentation distinguish the next stage. After that, the cell divides into membrane-bound, ultra-structurally preserved fragments that macrophages devour, decreasing inflammation. Forward and side scatter density plots are useful to identify your cell population of interest and remove debris. FSC versus SSC gating was used to identify cells that are intriguing based on size and detail (complexities). Forward scatter is frequently believed to indicate cell size, whereas side scatter symbolizes the cell's complexity or granularity. The SSC VS FSC plot was used to select the cell population in treated and unt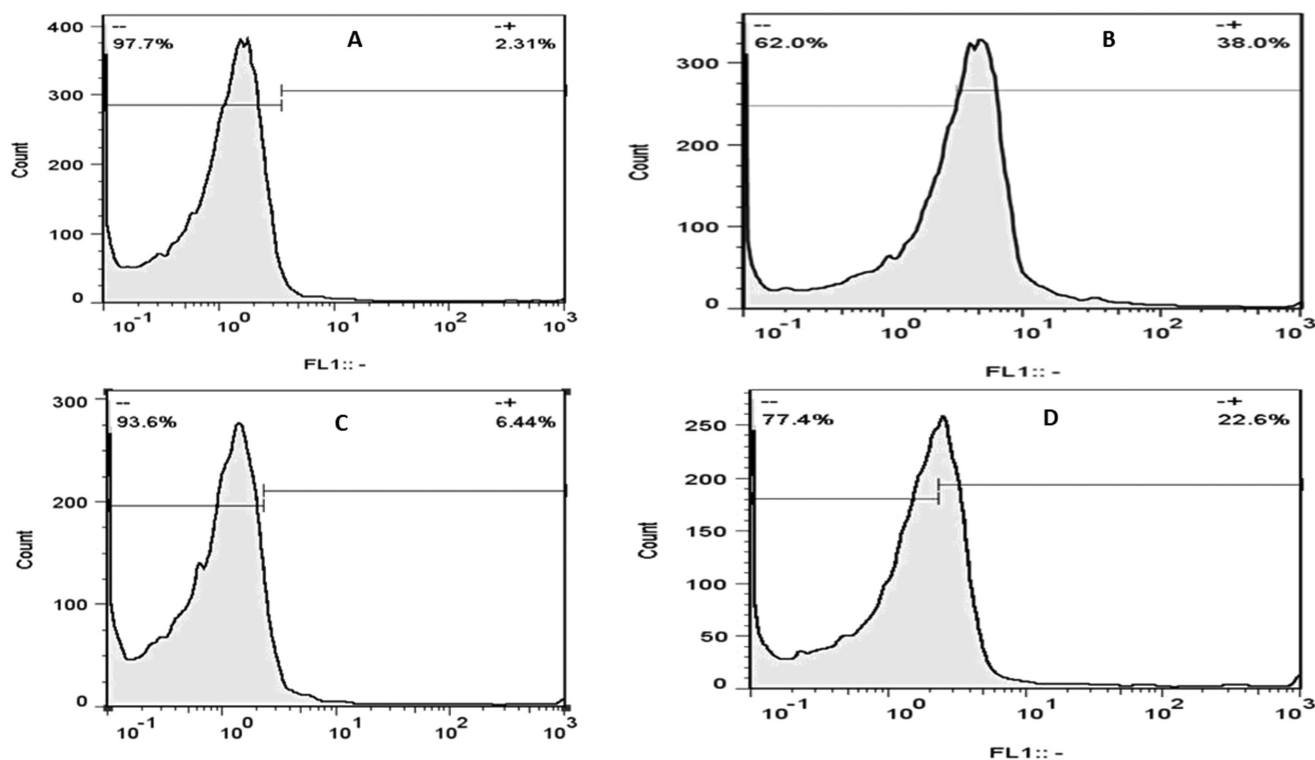reated cells for further investigation. The FL1 versus FL3 plot shows the state of the cell population that was gated with the aid of the FSC versus SSC plot. In brief, the FL1 versus FL3 plot is divided into 4 quartiles. The Q4 quartile shows the cell population that is stained neither with PI nor FITC-conjugated annexin. Therefore, the Q4 quartile shows the healthy cells that are nonapoptotic and non-necrotic. The Q3 quartile shows the cell population that is stained only with FITC-conjugated annexin and, therefore, is in the early stages of apoptosis. At the early stages of apoptosis, the integrity of the cell membrane is not jeopardized; therefore, PI stain is excluded from the cells. However, FITC-conjugated annexin binds to phosphatidylserines that are localized in the outer layer of the cytoplasmic membrane. The Q2 quartile represents the cell population that is stained with both PI and FITC-conjugated annexin and shows the cell population that is at the late stage of apoptosis, where the integrity of the cell membrane is disrupted, PI can easily penetrate the cell to stain the DNA, and phosphatidylserine is surfaced to bind annexin. The Q1 quartile shows necrotic cells. The necrotic cell's plasma membrane is disrupted, and PI stain can easily penetrate the cells, which also helps to remove debris and artifacts from the analysis. The IC_{50} value was used to determine early apoptosis (Q1), late apoptosis (Q2), necrosis (Q3), and cell survival (Q4). Untreated HepG2 cells showed early apoptosis

Figure 6

Flow cytometry analysis of silver nanofibers, showed apoptosis analysis: A. Untreated HepG2 cells. B. HepG2 cells treated with IC_{50} value of silver nanofibers. C. Untreated MDA-MB-231 cells. D. MDA-MB-231 cells treated with IC_{50} value of silver nanofibers.

Figure 7

Flow cytometry analysis of silver nanofibers, showed ROS analysis: A. Untreated HepG2 cells. B. HepG2 cells treated with IC_{50} value of silver nanofibers. C. Untreated MDA-MB-231 cells. D. MDA-MB-231 cells treated with IC_{50} value of silver nanofibers.

(0.804%), late apoptosis (0.190%), necrosis (3.39%), and living cells (95.6%), as shown in (Fig. 6a). Early apoptosis (0.00%), late apoptosis (0.095%), necrosis (60.6%), and living cells (39.3%) were seen in HepG2 cells treated with an IC_{50} value, Fig. 6b. Untreated MDA-MB-231 cells are seen in early apoptosis (0.375%), late apoptosis (0.112%), necrosis (2.48%), and surviving cells (97.0%) in (Fig. 6c). In MDA-MB-231 cells, the efficacy of apoptosis results indicated early apoptosis (0.045%), late apoptosis (0.015%), necrosis (16.4%), and life cells (83.6%) (Fig. 6d) [54,55].

Reactive oxygen species (ROS)
The IC_{50} values were utilized to evaluate the ROS results using flow cytometry. DCFH is used as a biomarker for ROS by comparing treated and untreated cells. This dye detects various ROS activities, such as hydroxyl and peroxyl radicals, within cells. Cellular esterases convert it into a non-fluorescent compound, which is subsequently oxidized by ROS to produce 2′, 7′-dichlorofluorescein (DCF). Even though DCFH is easily affected by light irradiation during measurements, it is still an important method for determining ROS levels in treated cells and comparing them to untreated cells to evaluate the efficacy of medications or plant extracts

because ROS plays a role in cell degradation. Untreated HepG2 cells (control) had 2.31% DCFH+, while cells treated with the IC_{50} value of AgNFs had 38.0% DCFH+, as shown in Fig. 7a–d show that untreated (control) MDA-MB-231 cells have (6.44%) DCFH+ and (22.6%) DCFH+ cells treated with AgNFs IC_{50} values. The count-FL1 plot is used to interpret the ROS production. In the treated cells, when compared to the control cells, the FL1 peak has shifted to the right. The more the peak shifts to the right, the more the cell population produces fluorescent light, which is proportional to an increase in ROS production [56,57].

Conclusion
The present research demonstrates that the essential oils of almond fruits can effectively contribute to the formation of AgNFs. SEM and FT-IR analyses confirmed the synthesis of AgNFs. Furthermore, the AgNFs showed antibacterial against Gram-negative bacteria *(P. aeruginosa and E. coli)*. Hence, AgNFs showed anticancer potential properties with HepG2 cells and MDA-MB-231 cells. The anticancer study revealed that AgNFs from almond oil could be developed in the future to protect against a variety of ailments. As a result, almond essential oils may be regarded as suitable ingredients for the manufacture of AgNFs, and this

methodology could serve as an environmentally friendly method of producing these AgNFs.

References

1 Magiorakos AP, Srinivasan A, Carey RB, Carmeli Y, Falagas ME, Giske CG, *et al.* Multidrug-resistant, extensively drug-resistant and pandrug-resistant bacteria: an international expert proposal for interim standard definitions for acquired resistance. Clin Microbiol Infect 2012; 18:268–281.

2 Ren Y yu, Yang H, Wang T, Wang C. Green synthesis and antimicrobial activity of monodisperse silver nanoparticles synthesized using Ginkgo Biloba leaf extract. Phys Lett A 2016; 380:3773–3777.

3 Riya P, Kumar SS, Giridhar P. Phytoconstituents, GC-MS Characterization of Omega Fatty Acids, and Antioxidant Potential of Less-Known Plant Rivina humilis L. ACS omega 2023; 8:28519–28530.

4 Manimaran M, Kannabiran K. Actinomycetes-mediated biogenic synthesis of metal and metal oxide nanoparticles: progress and challenges. Lett Appl Microbiol 2017; 64:401–408.

5 Bharathi D, Diviya Josebin M, Vasantharaj S, Bhuvaneshwari V. Biosynthesis of silver nanoparticles using stem bark extracts of Diospyros montana and their antioxidant and antibacterial activities. J Nanostructure Chem 2018; 8:83–92.

6 Bharathi D, Bhuvaneshwari V. Evaluation of the cytotoxic and antioxidant activity of phyto-synthesized silver nanoparticles using Cassia angustifolia flowers. Bionanoscience 2019; 9:155–163.

7 Behboodi S, Baghbani-Arani F, Abdalan S, Sadat Shandiz SA. Green engineered biomolecule-capped silver nanoparticles fabricated from Cichorium intybus extract: in vitro assessment on apoptosis properties toward human breast cancer (MCF-7) cells. Biol Trace Elem Res 2019; 187:392–402.

8 Logeswari P, Silambarasan S, Abraham J. Synthesis of silver nanoparticles using plants extract and analysis of their antimicrobial property. J Saudi Chem Soc 2015; 19:311–317.

9 Ibrahim HMM. Green synthesis and characterization of silver nanoparticles using banana peel extract and their antimicrobial activity against representative microorganisms. J Radiat Res Appl Sci 2015; 8:265–275.

10 Thawini HK, Al-Shawi AA. A polysaccharide of Ziziphus spina-Christi L., and it's Silver nanoparticles induced reactive oxygen species and late apoptosis of Liver cancer cells. Nanomedicine Res J 2021; 6:237–247.

11 Mostafa M, Kandile NG, Mahmoud MK, Ibrahim HM. Synthesis and characterization of polystyrene with embedded silver nanoparticle nanofibers to utilize as antibacterial and wound healing biomaterial. Heliyon 2022; 8:1.

12 Ferreira FV, Otoni CG, Lopes JH, de Souza LP, Mei LHI, Lona LMF, *et al.* Ultrathin polymer fibers hybridized with bioactive ceramics: A review on fundamental pathways of electrospinning towards bone regeneration. Mater Sci Eng C 2021; 123:111853.

13 Arida IA, Ali IH, Nasr M, El-Sherbiny IM. Electrospun polymer-based nanofiber scaffolds for skin regeneration. J Drug Deliv Sci Technol 2021; 64:102623.

14 Rickel AP, Deng X, Engebretson D, Hong Z. Electrospun nanofiber scaffold for vascular tissue engineering. Mater Sci Eng C 2021; 129:112373.

15 Cui C, Sun S, Wu S, Chen S, Ma J, Zhou F. Electrospun chitosan nanofibers for wound healing application. Eng Regen 2021; 2:82–90.

16 Zhao J, Liu Z, Low SC, Xu Z, Tan SH. Electrospinning technique meets solar energy: electrospun nanofiber-based evaporation systems for solar steam generation. Adv Fiber Mater 2023; 5:1318–1348.

17 Wang SX, Yap CC, He J, Chen C, Wong SY, Li X. Electrospinning: A facile technique for fabricating functional nanofibers for environmental applications. Nanotechnol Rev. 2016; 5:51–73.

18 Teo WE, Ramakrishna S. A review on electrospinning design and nanofibre assemblies. Nanotechnology 2006; 17:R89.

19 Uttara B, Singh AV, Zamboni P, Mahajan R. Oxidative stress and neurodegenerative diseases: a review of upstream and downstream antioxidant therapeutic options. Curr Neuropharmacol. 2009; 7:65–74.

20 Toncheva A, Spasova M, Paneva D, Manolova N, Rashkov I. Drug-loaded electrospun polylactide bundles. J Bioact Compat Polym. 2011; 26:161–172.

21 Passaro J, Imparato C, Parida D, Bifulco A, Branda F, Aronne A. Electrospinning of PVP-based ternary composites containing SiO2 nanoparticles and hybrid TiO2 microparticles with adsorbed superoxide radicals. Compos Part B Eng. 2022; 238:109874.

22 Fox ME, Szoka FC, Fréchet JMJ. Soluble polymer-carriers for the treatment of cancer: the importance of molecular architecture. Acc Chem Res. 2009; 42:1141–1151.

23 Wang X, Zhang X, Fu G, Tang Y. Recent progress of electrospun porous carbon-based nanofibers for oxygen electrocatalysis. Mater Today Energy. 2021; 22:100850.

24 Wang Y, Yokota T, Someya T. Electrospun nanofiber-based soft electronics. NPG Asia Mater. 2021; 13:22.

25 Nie G, Zhao X, Luan Y, Jiang J, Kou Z, Wang J. Key issues facing electrospun carbon nanofibers in energy applications: on-going approaches and challenges. Nanoscale. 2020; 12:13225–13248.

26 Zhang Z, Wu X, Kou Z, Song N, Nie G, Wang C, *et al.* Rational design of electrospun nanofiber-typed electrocatalysts for water splitting: A review. Chem Eng J. 2022; 428:131133.

27 Forghani S, Almasi H, Moradi M. Electrospun nanofibers as food freshness and time-temperature indicators: A new approach in food intelligent packaging. Innov Food Sci Emerg Technol. 2021; 73:102804.

28 Rinaldi F, Hanieh PN, Maurizi L, Longhi C, Uccelletti D, Schifano E, *et al.* Neem oil or almond oil nanoemulsions for vitamin E delivery: from structural evaluation to in vivo assessment of antioxidant and anti-inflammatory activity. Int J Nanomedicine. 2022; 17:6447.

29 Háková M, Havlíková LC, Švec F, Solich P, Šatínský D. Nanofibers as advanced sorbents for on-line solid phase extraction in liquid chromatography: A tutorial. Anal Chim Acta. 2020; 1121:83–96.

30 Liu J, Zhang F, Hou L, Li S, Gao Y, Xin Z, *et al.* Synergistic engineering of 1D electrospun nanofibers and 2D nanosheets for sustainable applications. Sustain Mater Technol 2020; 26:e00214.

31 de Souza PG, Rosenthal A, Ayres EMM, Teodoro AJ. Potential functional food products and molecular mechanisms of Portulaca oleracea L. on Anticancer Activity: A Review. Oxid Med Cell Longev. 2022; 2022: Article ID 7235412, 9 pages.

32 Gull N, Arshad F, Naikoo GA, Hassan IU, Pedram MZ, Ahmad A, *et al.* Recent advances in anticancer activity of novel plant extracts and compounds from Curcuma longa in hepatocellular carcinoma. J Gastrointest Cancer. 2023; 54:368–390.

33 Gao H, Yang H, Wang C. Controllable preparation and mechanism of nano-silver mediated by the microemulsion system of the clove oil. Results Phys. 2017; 7:3130–3136.

34 Burt S. Essential oils: their antibacterial properties and potential applications in foods—a review. Int J Food Microbiol. 2004; 94:223–253.

35 Hameed MF, Mkashaf IA, Al-Shawi AAA, Hussein KA. Antioxidant and Anticancer Activities of Heart Components Extracted from Iraqi Phoneix Dactylifera Chick. Asian Pac J Cancer Prev. 2021; 22:3533–3541.

36 Al-Shawi AAA, Hameed MF, Ali NH, Hussein KA. Investigations of Phytoconstituents, Antioxidant and Anti-Liver Cancer Activities of Saueda monoica Forssk Extracted by Microwave-Assisted Extraction. Asian Pac J Cancer Prev. 2020; 21:2349–2355.

37 Mericli F, Becer E, Kabadayı H, Hanoglu A, Yigit Hanoglu D, Ozkum Yavuz D, et al. Fatty acid composition and anticancer activity in colon carcinoma cell lines of Prunus dulcis seed oil. Pharm Biol. 2017; 55: 1239–1248.

38 Tlili N, Kirkan B, Sarikurkcu C. LC-ESI-MS/MS characterization, antioxidant power and inhibitory effects on α-amylase and tyrosinase of bioactive compounds from hulls of Amygdalus communis: The influence of the extracting solvents. Ind Crops Prod. 2019; 128:147–152.

39 Al-Shawi AAA, Hameed MF, Hussein KA, Neamah HF, Luaibi IN. Gas Chromatography-Mass Spectrometry Analysis of Bioactive Compounds of Iraqi Truffle Terfezia claveryi (Ascomycetes), Synthesis of Silver Nanoparticles, and Appraisal of Its Biological Activities. Int J Med Mushrooms. 2021; 23:79–89.

40 Sahiba N, Sethiya A, Agarwal DK, Agarwal S. An Overview on Immunity Booster Foods in Coronavirus Disease (COVID-19). Comb Chem High Throughput Screen. 2023; 26:1251–1284.

41 Vijayan R, Joseph S, Mathew B. Eco-friendly synthesis of silver and gold nanoparticles with enhanced antimicrobial, antioxidant, and catalytic activities. IET nanobiotechnology. 2018; 12:850–856.

42 Fernandes GD, Gómez-Coca RB, Pérez-Camino M del C, Moreda W, Barrera-Arellano D. Chemical characterization of major and minor compounds of nut oils: almond, hazelnut, and pecan nut. J Chem. 2017; 2017: Article ID 2609549, 11 pages.

43 Easawi K, Nabil M, Abdallah T, Negm S, Talaat H. Plasmonic absorption enhancement in Au/CdS nanocomposite. World Acad Sci Eng Technol. 2012; 6:25.

44 Abdallah T, El-Brolosy TA, Mohamed MB, Easawi K, Negm S, Talaat H. Effect of shape and interstice on surface enhanced Raman scattering (SERS) of molecules adsorbed on gold nanoparticles in the near-dipole and quadrupole regions. J Raman Spectrosc. 2012; 43:1924–1930.

45 Ahmad HS, Ateeb M, Noreen S, Farooq MI, Baig MMFA, Nazar MS, et al. Biomimetic synthesis and characterization of silver nanoparticles from Dipterygium glaucum extract and its anti-cancerous activities. J Mol Struct. 2023; 1282:135196.

46 Awwad J, Hammoud N, Farra C, Fares F, Abi Saad G, Ghazeeri G. Abdominal wall desmoid during pregnancy: diagnostic challenges. Case Rep Obstet Gynecol. 2013; 2013: Article ID 350894, 3 pages.

47 Akselband Y, Cabral C, Shapiro DS, McGrath P. Rapid mycobacteria drug susceptibility testing using Gel Microdrop (GMD) Growth Assay and flow cytometry. J Microbiol Methods. 2005; 62(2):181–197.

48 Jorgensen JH, Ferraro MJ. Antimicrobial susceptibility testing: a review of general principles and contemporary practices. Clin Infect Dis. 2009; 49(11):1749–1755.

49 Ahmed S, Ahmad M, Swami BL, Ikram S. A review on plants extract mediated synthesis of silver nanoparticles for antimicrobial applications: a green expertise. J Adv Res 2016; 7:17–28.

50 de Santa Maria LC, Santos ALC, Oliveira PC, Barud HS, Messaddeq Y, Ribeiro SJL. Synthesis and characterization of silver nanoparticles impregnated into bacterial cellulose. Mater Lett. 2009; 63:797–799.

51 Feng QL, Wu J, Chen GQ, Cui FZ, Kim TN, Kim JO. A mechanistic study of the antibacterial effect of silver ions on Escherichia coli and Staphylococcus aureus. J Biomed Mater Res 2000; 52:662–668.

52 Morones JR, Elechiguerra JL, Camacho A, Holt K, Kouri JB, Ramírez JT, et al. The bactericidal effect of silver nanoparticles. Nanotechnology. 2005; 16:2346.

53 Bharathi D, Vasantharaj S, Bhuvaneshwari V. Green synthesis of silver nanoparticles using Cordia dichotoma fruit extract and its enhanced antibacterial, anti-biofilm and photo catalytic activity. Mater Res Express 2018; 5:55404.

54 Sabapathi N, Ramalingam S, Aruljothi KN, Lee J, Barathi S. Characterization and Therapeutic Applications of Biosynthesized Silver Nanoparticles Using Cassia auriculate Flower Extract. Plants. 2023; 12:707.

55 Mani M, Okla MK, Selvaraj S, Kumar AR, Kumaresan S, Muthukumaran A, et al. A novel biogenic Allium cepa leaf mediated silver nanoparticles for antimicrobial, antioxidant, and anticancer effects on MCF-7 cell line. Environ Res. 2021; 198:111199.

56 Mohanpuria P, Rana NK, Yadav SK. Biosynthesis of nanoparticles: technological concepts and future applications. J Nanoparticle Res 2008; 10:507–517.

57 Song JY, Kim BS. Rapid biological synthesis of silver nanoparticles using plant leaf extracts. Bioprocess Biosyst Eng. 2009; 32:79–84.